Porosity estimation of a micro-cracked adhesive interface by μCT scanning: Comparison between experimentally measured effective stiffnesses and those predicted by an imperfect interface model

M. Lamberti, Aurelien Maurel-Pantel, K. Idrissa, F. Lebon

Porosity estimation of a micro-cracked adhesive interface by µCT scanning: comparison between experimentally measured effective stiffnesses and those predicted by an imperfect interface model.

M. Lamberti, A. Maurel-Pantel*, K. Idrissa, F. Lebon

Aix Marseille Univ, CNRS, Centrale Marseille, LMA, Marseille, France

**Corresponding author :*

Aurélien Maurel-Pantel

Laboratoire de Mécanique et d'Acoustique

4 impasse Nikola TESLA CS 40006 13453 MARSEILLE CEDEX 13

email: maurel@lma.cnrs-mrs.fr

Abstract

The presence of defects in adhesive materials influences the mechanical behaviour of bonded composite structures. Indeed, the initial defects in the adhesive joint damage the mechanical properties of the interface and reduce the mechanical strength of the structure.

An in-depth study of the influence of initial porosity in the bonded joints on the mechanical properties of the rigid adhesive material has been experimentally measured. Different joint geometries are investigated by varying the thickness and the bonding area. A modified Arcan device is used to load the bonds in tension (initiation in Mode I). An imperfect interface model capable of considering the presence of initial diffuse cracks according to the Kachanov-Sevostianov material definition is then used to predict the mechanical properties of these adhesive joints. In this model, the presence of defects in the adhesive layer is described by an initial damage parameter: the porosity rate. Prior to testing, the porosity rates of the bonded joints are measured using μCT scans. Finally, the mechanical properties obtained experimentally are compared with those predicted by the imperfect interface model.

Keywords: Adhesive bonding, CT-scans, Damage, Porosity, Kachanov-Sevostianov's material

1. Introduction

Over the last decade, the use of adhesives in the mechanical and civil engineering sectors has grown exponentially due to their ability to easily and quickly bond different types of materials such as steel, aluminium, masonry and composites. The use of adhesive bonding in various industrial sectors is increasing significantly due to the increasing demand for the design of lightweight structures such as aircraft and vehicle body frames. Due to this factor, the joining techniques for joining advanced lightweight materials that are dissimilar, coated and difficult to weld have been thoroughly investigated in recent years [1]. Although adhesive bonding has been used as a traditional joining method for many centuries, it is only in the last seventy years that the science and technology of adhesive bonding has really progressed significantly [2].

In addition to civil engineering, the bonding technique has been increasingly used in structural strengthening and reinforcement of concrete elements by adding FRP sheet material, both in fully composite structures such as pedestrian bridges and in buildings where pultruded profiles have been joined together to form more complex cross-sections [3]. Moreover, the joints of this type are particularly suitable for the realisation of secondary structures such as parapets, stairs, railings in various types of construction; buildings, cooling towers and offshore installations. For these reasons, there has been a great interest in the scientific and industrial communities to have tools capable of describing and simulating the behaviour of adhesive bonds. Several approaches have been proposed in the literature to describe the behaviour of the bonded interface for different types of applications using analytical or finite element models. In these models, the description of damage is increasingly studied in order to simulate the loss of elastic properties of the interface, to simulate the evolution of these properties during the lifetime of the structure and to describe the failure processes of the assemblies. The most important characteristics for bonded joints to predict their mechanical performance are undoubtedly the stiffness and stress at failure of the bonded interface.

In the framework of continuum damage mechanics, internal damage can be assessed indirectly by the variation of material properties such as elastic coefficients [4,5]. A recent review of the subject is presented in [6], from the initial papers of Kachanov [7] and Rabotnov [8] to the most recent work, with emphasis on continuum damage of concrete and plasticity modelling. Fundamental aspects of damage mechanics with new derivations and remarks have recently been presented in the review [9]. Numerical aspects of continuum damage mechanics, with special emphasis on mesh sensitivity, are reviewed in [10]. A recent continuous damage approach, based on the continuous-time fatigue model of Ottosen et al [11], is proposed in [12], where an analytical solution for the evolution of damage

due to cyclic proportional loading is also given. The proposed approach has also been implemented in continuous-time topological optimisation fatigue problems [13]. Damage modelling techniques can be divided into either local or continuum approaches. In the continuum approach, damage is modelled over a finite region, whereas in the local approach, damage is restricted to zero volume lines and surfaces and is often referred to as the cohesive zone approach [14].

Another approach is to use spring type imperfect interface models. These models are derived by introducing a stress-based micromechanical homogenisation [15-18,19] to treat the damaged interphase within the matched asymptotic expansion method. The interface model is formulated assuming a three-dimensional isotropic interphase weakened by penny-shaped microcracks according to the Kachanov-Sevostianov material definition. The Kachanov-Sevostianov (KS) theory [15] consists in considering the presence of initial cracks inside an adhesive material. The main assumptions of the microcracked adhesive are the following: non-interaction between the crack, a constant stress vector along the crack and the effect of the crack edge in the stress field are ignored. Furthermore, the peculiarity of this model is that it takes into account some of the most important bond variabilities such as thickness variation, porosity and initial damage [16,20]. The KS type model has previously been successfully applied to cracked to foamed aluminium [16], composite materials [20] and masonry structures [21]. The accuracy of this model, which generally depends on the density of the cracks, is satisfactory up to quite small distances between cracks (distances much smaller than the crack width). The KS model includes a global parameter called the crack density, which is defined by the number and length of all cracks.

In this paper the influence of initial porosity in the bonded joint on the mechanical properties of the rigid adhesive material Sikadur-30 [22] is measured experimentally. The initial defects affect the mechanical properties of the interface and thus the mechanical strength of the structure. In a first part, the mechanical properties of the adhesive are determined by tensile tests. In a second part, different joint geometries are investigated by varying the thickness and the bonding area. A modified Arcan device is used to test the bonded specimens in Mode I. Prior to testing, the porosity rates of the bonded joints are measured using μCT scans. In a third section, an imperfect interface model capable of accounting for the presence of initial diffuse cracks according to the Kachanov-Sevostianov material definition is then used to predict the mechanical properties of adhesive joints. In the model, the presence of defects in the adhesive layer is described by an initial damage parameter: the porosity rate. Finally, the mechanical properties obtained experimentally are compared with those predicted by the imperfect interface model.

2. Experimental characterization of the adhesive

2.1 Adhesive

The adhesive used is an epoxy two-component adhesive names Sikadur-30, available on the market and produced by Sika [23]. The two-component thixotropic structural adhesive reaches the strength capacity after the polymerisation process between a mixture of epoxy resin and special fillers, which ends after a curing of 7 days at temperatures ranging from 8° to 35°. The mechanical properties declared by the manufacturer are given in Table 1.

Table 1. Mechanical properties of the epoxy adhesive (SikaDur-30).

	Value
Young's Modulus in compression, E_C	9600MPa
Young's Modulus in tension, E_T	11200 MPa
Compressive Strength, σ_C	70-80 MPa (at 15°C) and 85-95 MPa (at 35°C)
Tensile Strength, σ_N	24-27 MPa (at 15°C) and 26-31 MPa (at 35°C)
Shear Strength, τ	14-17 MPa (at 15°C) and 16-19 MPa (at 35°C)

2.2 Tensile test on the adhesive

Tensile tests have been set up to evaluate the Young's modulus and Poisson's ratio of Sikadur-30 adhesive. The resin is mixed with the hardener by hand at room temperature (about 25°C). After preparation is placed in a Teflon mould waiting the polymerisation process. The adhesive sheets are removed from the mould after 7 days, as shown in Figure 1. Four samples are then cut into each sheet using a water jet cutting machine.

a)

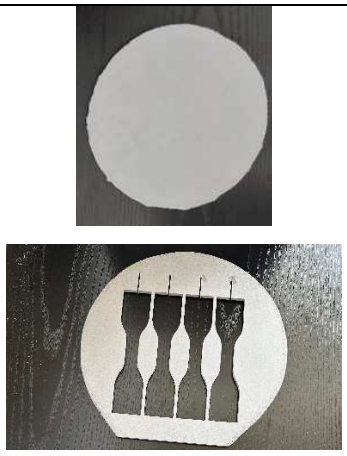

b)

Fig.1. Mould in Teflon used to make the sheets of adhesive material (a) before machining the specimens by water jet machining (b).

a)

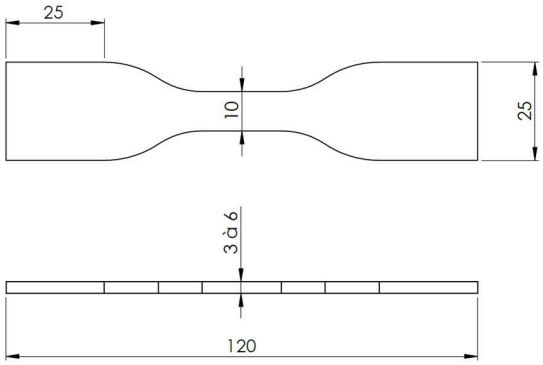

b)

Fig.2. Experimental setup for obtaining the stress-strain curve using digital image correlation technique. (b) Geometry of the tensile specimens (dimensions in mm).

The static tensile tests were carried out at the Mechanical and Acoustic Laboratory of the CNRS in Marseille using a universal tensile machine MTS 322 with a load capacity of 100 kN. The tests were performed under displacement control at a quasi-static rate of 0.5 mm/min. The strain field is measured using a digital image correlation technique. Images of the specimens are taken at regular intervals (15Hz frequency) during the test using a PCO.edges CMOS camera equipped with a 5.5 megapixel sensor. The images are then analysed using the GOM ARAMIS 6.5 Direct Image Correlation (DIC) software to determine the stress-strain curves of the specimen. The setup is shown in Figure 2a. The tensile test specimens were selected with the geometric dimensions shown in Figure 2b.

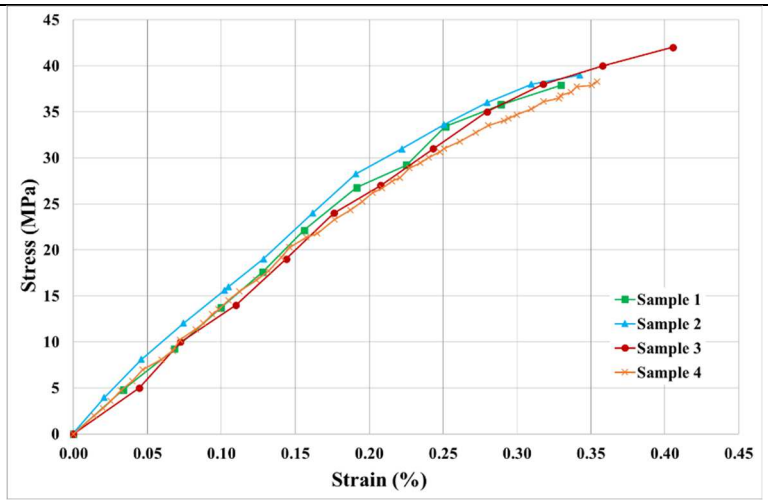

Fig.3. Evolution of stresses as a function of strain for specimens of SIKADUR 30 adhesive.

Figure 3 shows the stress-strain curves up to failure. As expected, the adhesives exhibit elastic behaviour, slightly non-linear (due to damage evolution), up to brittle fracture. The Young's modulus, ultimate tensile stress and Poisson's ratio of the SikaDur-30 adhesive are measured and reported in Table 2. These results are close to those quoted by the manufacturer (Table 1).

Table 2. Mechanical properties of SikaDur-30 adhesive measured experimentally.

Young's Modulus E_T (MPa)		**Tensile Strength σ_N (MPa)**		**Poisson's Ratio ν**	
Average value	Standard Deviation	Average value	Standard Deviation	Average value	Standard Deviation
11086	757.88	38.75	1.27	0.21	0.01

3. Experimental characterization of bonded specimens

3.1 Bonding protocol

The bonded specimens are realised by joining two cylindrical elements in aluminium 2017 using SikaDur-30 adhesive. The mechanical properties of the aluminium material are summarised in Table 3.

Table 3. Mechanical Properties of Aluminium 2017.

	Value
Young's Modulus, E_A	70 GPa
Poisson's ratio, ν_A	0.3

The bonded specimens were made to keep constant the total height, t_{tot}, equal to 64 mm, given by the sum of the adhesive thickness t_a, and the two cylindrical aluminium parts, t_{al}, both variable in the present experimental study (Figure 4).

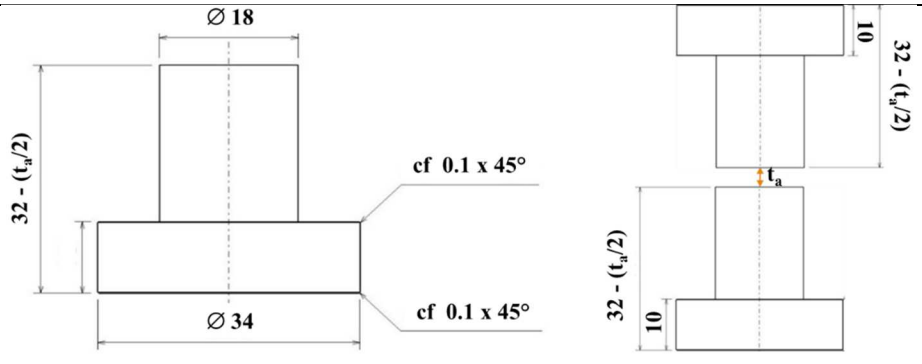

Fig.4. Cylindrical samples used for the mechanical tests.

(a)

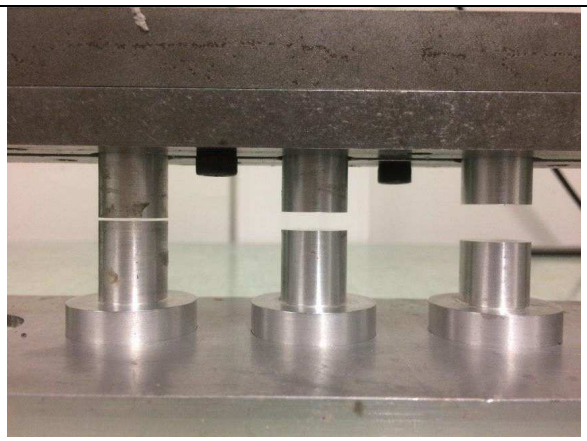

(b)

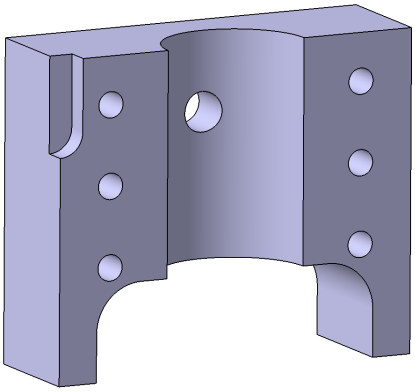

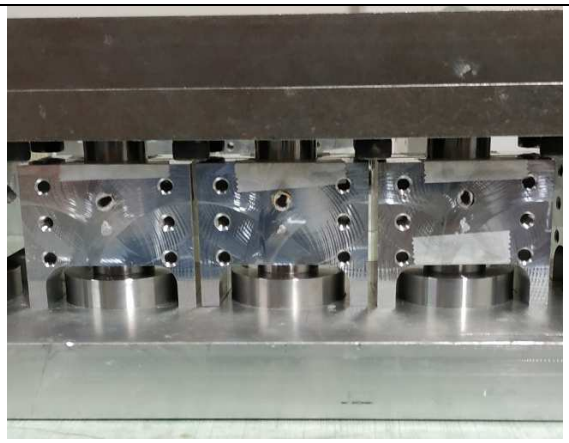

(c)

Fig.5. Mounting device for checking coaxiality and adhesive thickness (a-b).

Before bonding, to ensure the bonding effectiveness and to reduce measurement dispersion, the bonding surface quality is controlled by imposing a surface finish as the manufacturing final step. The specified surface roughness R_a is chosen to be equal to 0.1 µm. The aluminium surfaces are then perfectly cleaned with acetone. In order to achieve co-axiality between the two cylindrical aluminium parts, a mounting system was used as shown in Figure 5 (a) and Figure 5 (b).

The mounting device contains five semi-cylindrical parts, allowing more samples to be made at the same time. Initially, the aluminium parts are placed on the lower base and the adhesive mixture can be applied to the cylindrical surface. The other five aluminium halves are flanged into the fixture to facilitate positioning and promote co-axiality. A guide system allows the upper base to be positioned on the lower base and the thickness between the cylindrical samples to be calibrated. Once the mounting system has been assembled, it is necessary to wait seven days for the adhesive layer to polymerise completely at room temperature before removing the specimens. In order to achieve perfect control of the adhesive joint and better control the defects, an aluminium part, described in Figure 5 (c), was developed to calibrate the cylindricity of the adhesive joint and reduce its porosity. The part is covered with Teflon tape, and two parts are assembled on either side of the adhesive joint. Two holes allow the operator to inject the glue and evacuate the surplus. After a few hours of polymerisation, the parts are removed. A total of 60 samples of different adhesive thickness and surface were tested. Three different surfaces were considered, corresponding to diameters of 18, 14 and 10 mm respectively, and four different adhesive thicknesses, corresponding to 1, 2.5, 5 and 10 mm respectively. For each configuration, a minimum of five samples were tested to ensure an acceptable statistic.

3.2 Evaluation of adhesive joint porosities with µCT scans

In this section, the initial volumes of porosity in each bonded specimen are measured using µCT scans before to be tested. The bonded joints are scanned integrally using an X-ray source with a voxel size of 11 µm, a voltage of 150 Kev and a current of 200 µA. The imager has a resolution of 1920 x 1536 pixels. The device used is an EasyTom XL Ultra 150/160 (µCT) manufactured by RX Solution. Figure 6 describes how the sample is placed in the tomograph machine.

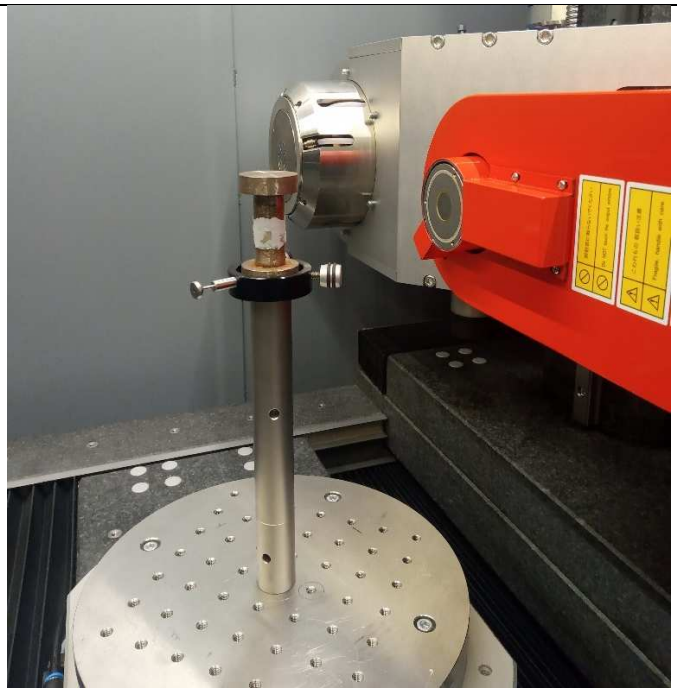

Fig.6. Bonded specimen placed in the X-ray microtomograph chamber of the EasyTom XL Ultra 150/160 (µCT) manufactured by RX Solution

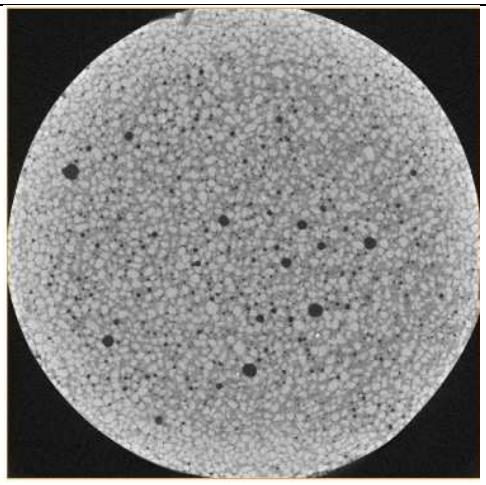

(a) D14T1

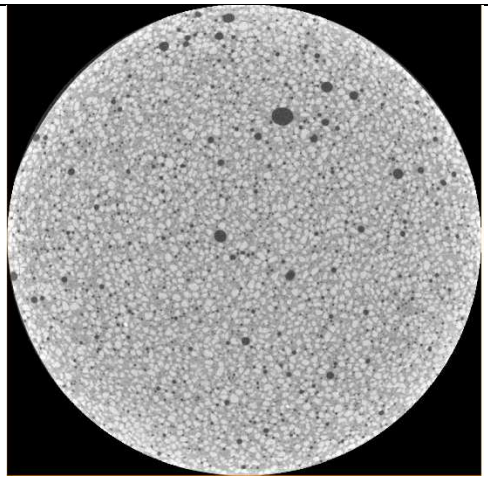

(b) D18T10

Fig.7. Vertical slices of the adhesive joint of the bonded specimens

At the end of the reconstruction, each slice of the µCt scan obtained has the thickness of a voxel (11 µm). Sikadur-30 is a filled adhesive, on the slice image the binders can be seen in grey, the colloidal fillers in white and the pores with the lower density appear in black, as shown in Figure 7. In these 3D CT scan images, diffuse porosity is observed for each thickness and diameter of the bond.

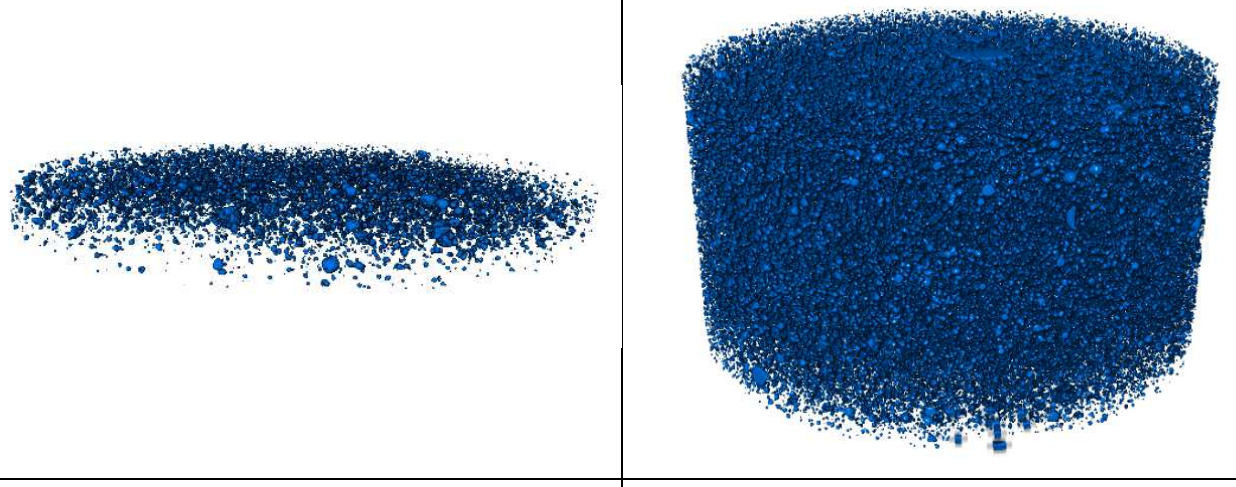

(a) D14T1	(b) D18T10

Fig.8. Three-dimensional images of the porosity present in two adhesive joints of bonded samples of different geometries: (a) diameter of 14 mm and adhesive thickness of 1 mm; (b) diameter of 18 mm and adhesive thickness of 10 mm;

In any case, it is difficult to make a quantitative assessment by looking only at the slices obtained by microtomography. To obtain a more quantitative measurement, the stack of slices is uploaded to an open source analysis software called Imorph [24]. This software allows to perform the segmentation between pores and adhesive matrix. The void phase described by the pores spatial distribution can be observed in Figure 8. Then the software allows to construct the boundary surfaces of the two phases and to calculate a porosity rate ρ in the volume of the joint V.

Figure 8 shows the 3D reconstruction of the pores obtained by the software for three different diameters of the adhesive samples. The number of pores appears to be very diffuse and visually quite important. The software is then able to quantify the volume of each phase. The values of the porosity rates calculated for the three thicknesses are given in Table 4. The average value of the porosity rate noted ρ seems to be independent of the bond surface or thickness. The value is constant around 5% and seems to be a specific property of the Sika Dur-30 adhesive and perhaps a consequence of the bonding process.

Table 4. Porosity rate of bonded joints measured by µCT scanning (5 samples per condition).

Diameter (mm)	Thickness (mm)	Volume (mm^3)	ρ (%)	
			Average value	Standard deviation
10	1	78.54	5.05	0.99
	2.5	196.35	5.53	0.27
	5	392.7	5.31	0.43
	10	785.4	5.48	0.91
14	1	153.94	5.33	1.07
	2.5	384.85	5.00	0.26
	5	769.69	5.26	0.71
	10	1539.38	5.51	0.23
18	1	254.47	5.35	0.5
	2.5	636.17	5.1	0.96
	5	1272.35	5.95	1.35
	10	2544.69	5.09	0.55

3.3 Experimental set-up

The experimental tensile static tests were carried out using the modified Arcan device with cylindrical specimens [25]. The device is made up of two half disks characterised by several attachment points along the circumference. These attachment points allow the device to be mounted on a standard tensile testing machine. The external flanges are used to position the specimen and are fastened by means of class 12.9 steel screws evenly distributed on the disk. To maintain a good stiffness gap, the vertical half discs are made of 40CMD8 steel and the horizontal flanges are made of 7075 aluminium. A 3D CAD design of the Arcan unit is shown in Figure 9.

The static tensile tests were performed at the Mechanical and Acoustic Laboratory of the CNRS in Marseille using a universal tensile machine called "MTS 322 test frame" with a load capacity of 100 kN. The tests were carried out under displacement control at a quasi-static rate of 1 mm/min. The Arcan device was connected to the machine by means of a ball-and-socket joint capable of ensuring isostatism and alignment of the applied load (see Figure 10).

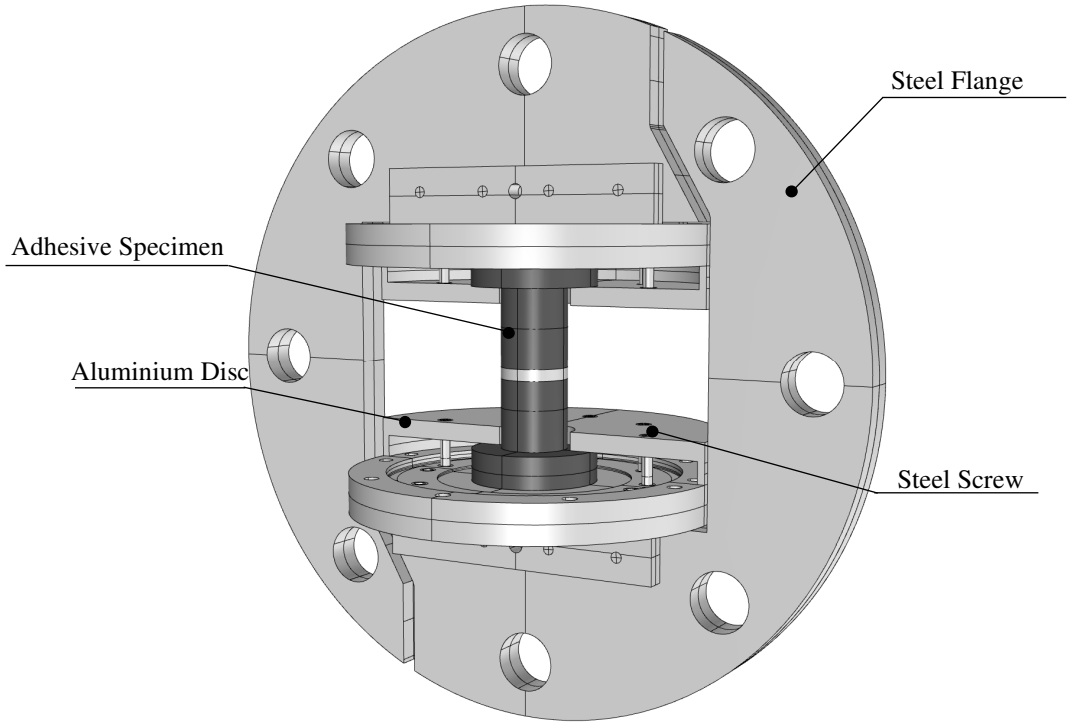

Fig.9. Arcan modified device for the test specimens (3D view)

a)

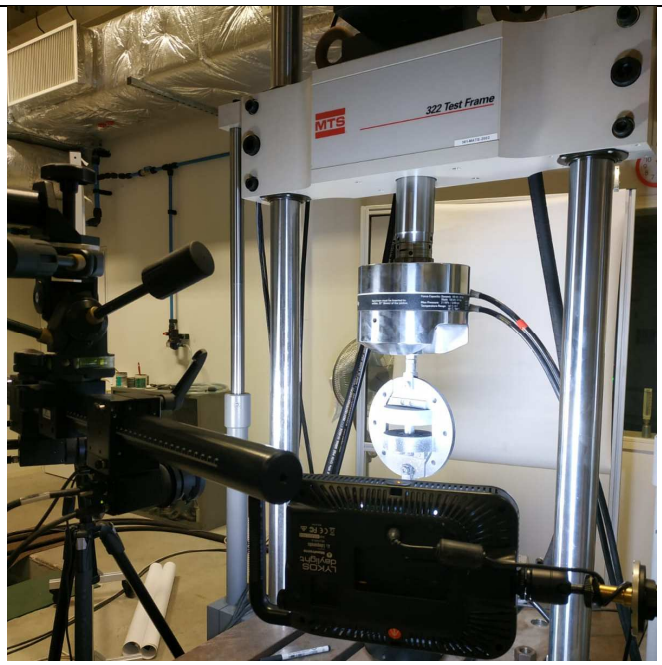

b)

Fig.10. Arcan device in the MTS 322 universal testing machine: a) Tensile load application; b) DIC system

A 3D DIC system was installed to evaluate the displacements and strains of the adhesive interface. During the experimental tests, the corresponding displacement and strain measurements of the adhesive thickness are continuously acquired by processing in-situ images taken by a DIC system from one side. A camera monitors the adhesive layer of the specimen during the loading process.

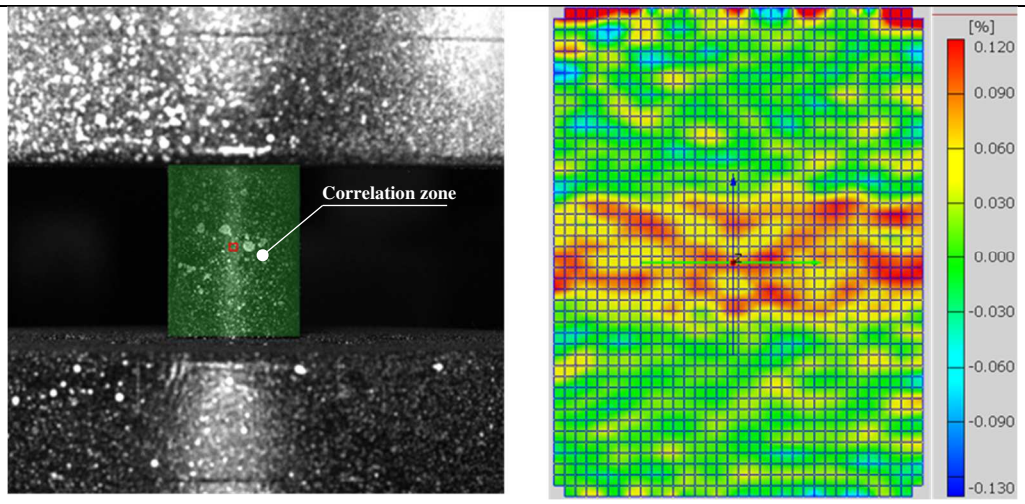

Fig.11. 3D DIC Analysis using Aramis software on cylindrical bonded samples

The strains are measured using an optical extensometer technique. The images are then analysed using the GOM ARAMIS 6.5 Direct Image Correlation (DIC) software, two points on the coupon surface are selected and the differential displacement between them is used to estimate the deformation of the specimen. The Aramis software was used to acquire the speckle pattern images from the camera. The acquisition frame rate was set to 3 frames per second (fps) for the uniaxial tensile test. The speckle pattern images acquired by the camera were then processed using the Aramis software. When processing these images, the subset size was set to 15 x 15 pixels. Global mean strain values (ε_{xx}; ε_{yy}; ε_{xy}) are obtained from the DIC analysis using Aramis software, an example is reported in Figure 11.

Figures 12 to 15 show the experimental failure mode (i.e. crack propagation in the adhesive joint) observed using a camera in the correlation zone described in Figure 11. As can be seen also in Figure 16, the failure mode in all specimens was cohesive, with the fracture propagating within the adhesive layer.

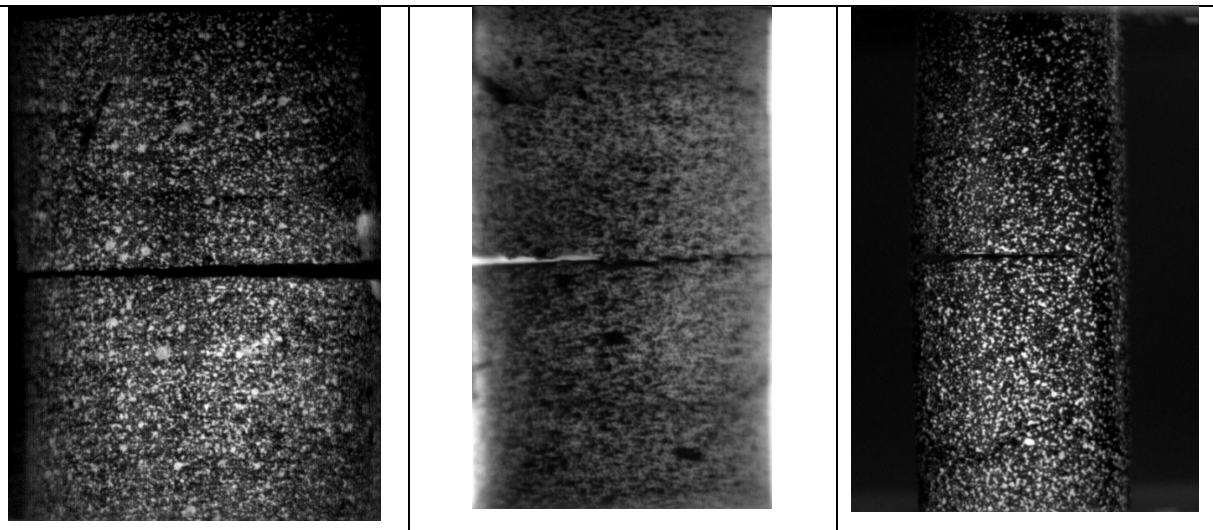

a)	b)	c)

Fig.12. Failure mode for 1 mm thick specimens: a) D18; b) D14; c) D10

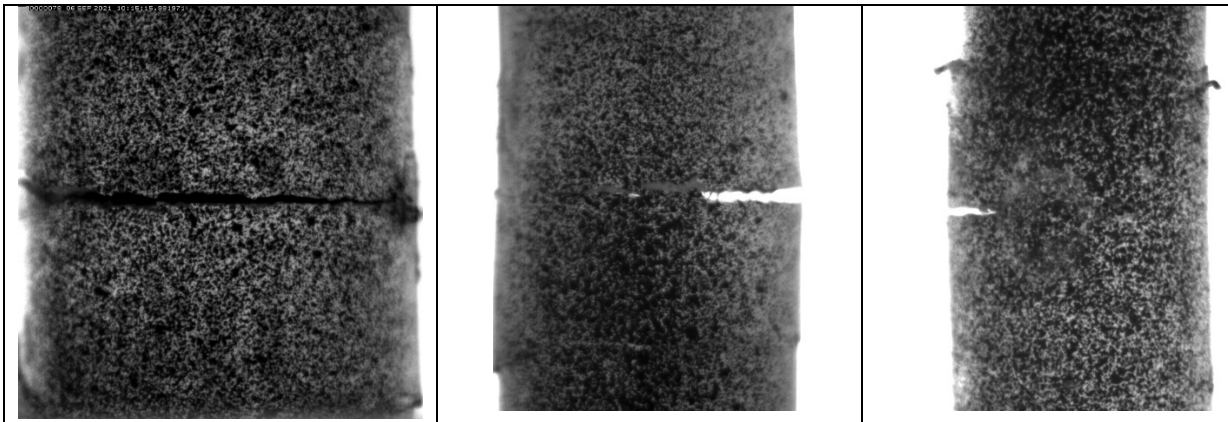

a)	b)	c)

Fig.13. Failure mode for 2.5 mm thick specimens: a) D18; b) D14; c) D10

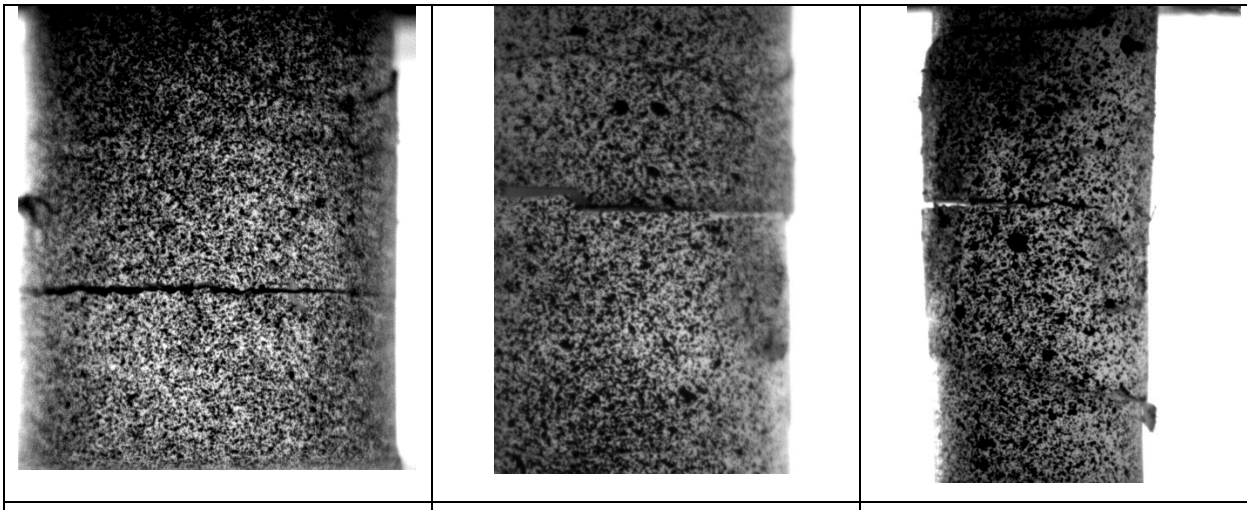

a)	b)	c)

Fig.14. Failure mode for 5 mm thick specimens: a) D18; b) D14; c) D10

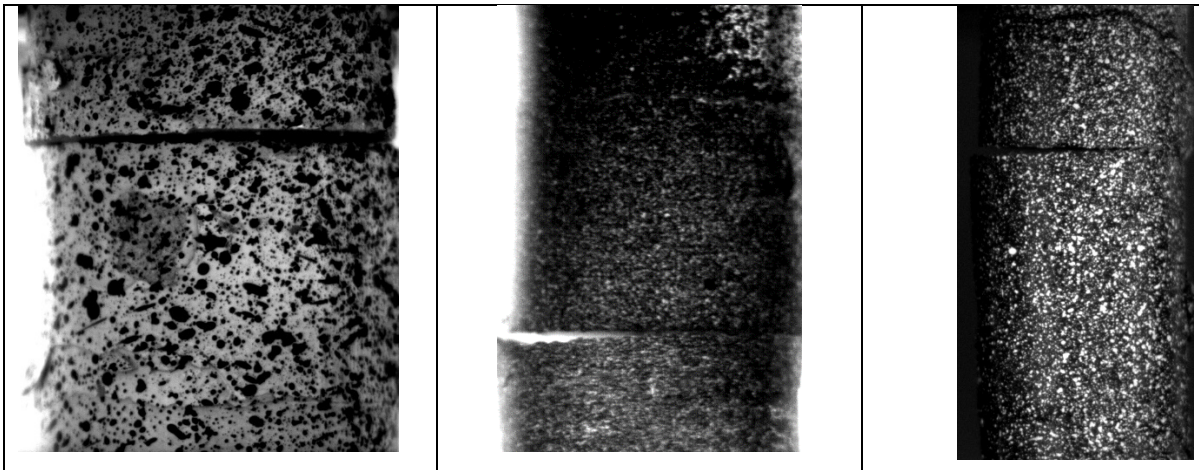

a)	b)	c)

Fig.15. Failure mode for 10 mm thick specimens: a) D18; b) D14; c) D10

Fig.16. cohesive failure of a specimen with a diameter of 18 mm and a thickness of 5 mm

3.4 Experimental results

The experimental results for each thickness are given in Table 5. The identification label has the generic form "D-T", where "D" and "T" denote the bonded area relative to a diameter of 18 mm (D18), 14 mm (D14) and 10 mm (D10), respectively, and the bond thickness (1, 2.5, 5, 10 mm). Table 5 shows for each specimen its measured values of normal stress at failure, σ_u and normal stiffness K_N, characterised by the specimen stress-strain curve.

Table 5 – Experimental results: stiffness K_N and normal stress at failure of bonded specimens

Test ID	K_N (N/mm^3)		σ_u (MPa)	
	Average value	Standard deviation	Average value	Standard deviation
D10T1	510	29.7	30.1	3.9
D10T2.5	464.6	32.3	18.5	4.1
D10T5	390	10.5	17.7	3.4
D10T10	202.3	56.5	13	2.9
D14T1	334.1	32.6	36	13
D14T2.5	307.7	25.2	25.4	0.9
D14T5	309.0	39.6	17.7	1.9
D14T10	288	12.7	21.3	4.1
D18T1	219.3	17.5	30.1	1.5
D18T2.5	204.1	17.1	22.1	0.1
D18T5	199.1	22.1	19.7	2.0
D18T10	184	20.0	16.2	0.4

Figure 17c describes the average normal stress at failure as well as the standard deviation of the bonded joints for the 18 mm diameter surface at varying adhesive thicknesses (1, 2.5, 5, 10 mm). For the D18T1 specimens, the average normal stress is higher with respect to those of the other thicknesses and seems to decrease as a function of the thickness, as expected. For this diameter it was observed a very low dispersion.

Figures 17a and 17b describe the average of the normal stress at failure as well as the standard deviation of the bonded joints for the 14 mm and 10 mm diameter surfaces at varying adhesive thickness (1, 2.5, 5, 10 mm). For both surfaces the trend of the normal stress at failure at varying adhesive thickness follows the same behaviour as previously discussed (D18). The decrease in diameter seems to increase the scatter in the experimental results.

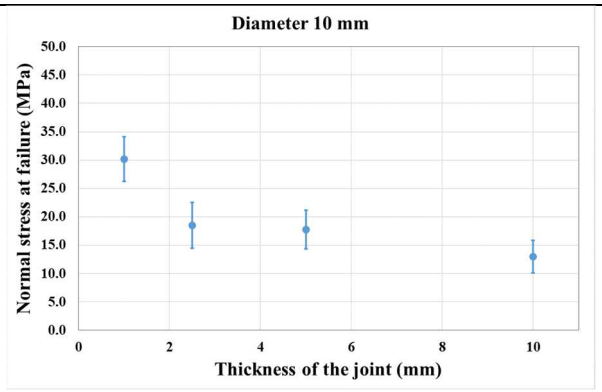

(a)

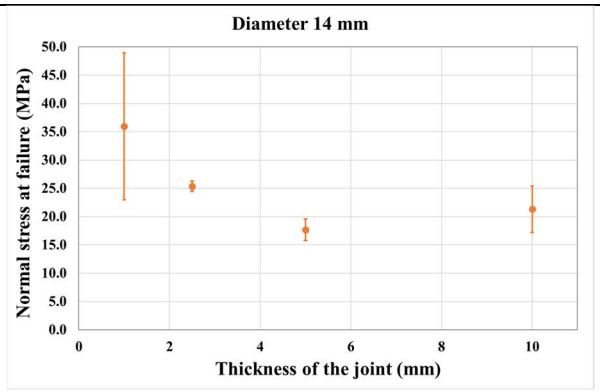

(b)

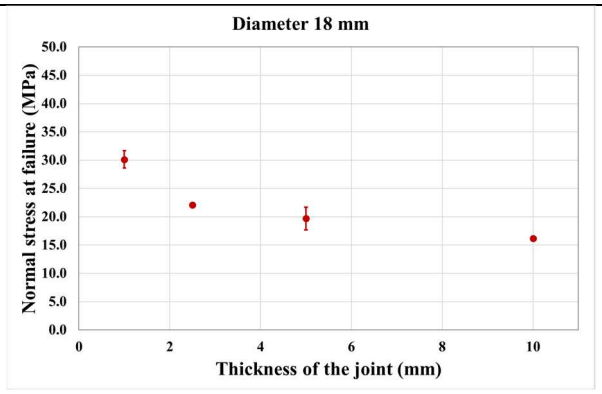

(c)

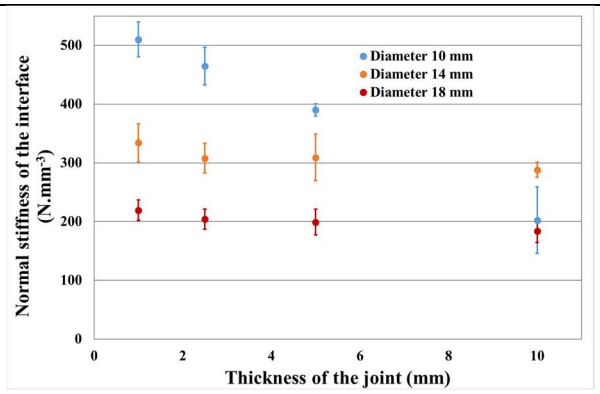

(d)

Fig.17. (a), (b) and (c) show the average normal stress at failure and the standard deviation of the bonded joints for a 10 mm, 14 mm and 18 mm diameter area for different adhesive thicknesses (1, 2.5, 5, 10 mm) respectively. (d) give the average normal stiffness KN of the interface for each geometric condition tested.

Finally, in Figure 17d, the average normal stiffness K_N of the interface is calculated with its standard deviation. The results show that the normal stiffness decreases with increasing thickness for each adhesive surface and also decreases with increasing surface area of the interface. For D18 the effect seems to be less important, and the value is almost constant. This leads to the conclusion that the normal stiffness of the interface is influenced by the geometric dimension of the bonded joint. [26-28]

4. Imperfect interface model

In the previous sections, several mechanical parameters of the epoxy adhesive and the bonded assembly have been measured and discussed. Two parameters are of great interest: the elastic properties of the adhesive and its porosity. In this section, the authors propose an imperfect interface model able to describe the properties of an adhesive joint with initial damage (initial porosity), in which these two parameters are useful for predicting the stiffness of the bonded assembly.

4.1 Initial damage property of Kachanov's material

The main idea is to define the model from a homogenised material containing microcracks. The microcrack density is assimilated to the porosity parameter using µCT scans. Among the different possibilities existing in the literature, we have chosen the Kachanov-Sevostianov (KS) model [15,16,20], which has the advantage of being a simple and efficient model as demonstrated in literature [22]. According to the Kachanov-Sevostianov theory, the description of the material starts from the evaluation of its initial damage. For this material, the effect of a given number of diffuse cracks can be assumed as the effect of a single large crack, which is able to describe the loss of adhesive stiffness as a function of the initial crack rate. In general, the KS model is of the form:

$$K = \frac{K_0}{1+C\rho} \tag{1}$$

Where K_0 is the initial parameter (stiffness, viscosity, etc.), K the "damaged" parameter, ρ the crack density and C a parameter that depends on the material and the on the shape of the crack. Classically,

$$\rho = 100 \times \frac{l^3}{V} \tag{2}$$

Where l is the representative crack-length and V the volume of material. Note that in practice ρ is measured in %. The thickness of the adhesive is usually small (noted as ε). Following the asymptotic technique presented in [29,30], the parameter $\varepsilon = \frac{\rho S}{100\, l^3}$, where S corresponding to the bonding surface) can be eliminated by going to the limit. An imperfect interface model is then obtained (hereafter referred to as the KSi model). The mechanical parameters depend on the crack-length. For example, the normal stiffness is given by:

$$K_N = \frac{3E_0 S}{16\, l^3 100(1-\nu_0^2)} \tag{3}$$

Where $E_0$is the Young's modulus and ν_0 the Poisson's ratio of the adhesive. Note that an evolution law of l can be added (see [31-33]). Details of the method are given in Appendices 1 and 2.

4.2 Prediction with the KSi model versus experimentally measured values

The µCT scans have shown the existence of an initial porosity in the adhesive joint, which can be considered as an initial damage. The KSi model can be used to predict the normal stiffness of the joint, the values are related in Table 6. From the experimental results described in the previous section, The Young's modulus E, the Poisson's ratio ν both are reported in Table 2 and the porosity rate is reported in Table 4. These parameters can be used to evaluate the normal stiffness of the joint.

Table 6 Stiffness K_N of adhesively bonded specimens predicted with KSi model

Test ID	K_N (N/mm^3)
D10T1	430.3
D10T2.5	157.3
D10T5	81.9
D10T10	39.6
D14T1	407.8
D14T2.5	174.0
D14T5	82.7
D14T10	39.4
D18T1	406.1
D18T2.5	170.7
D18T5	73.1
D18T10	42.7

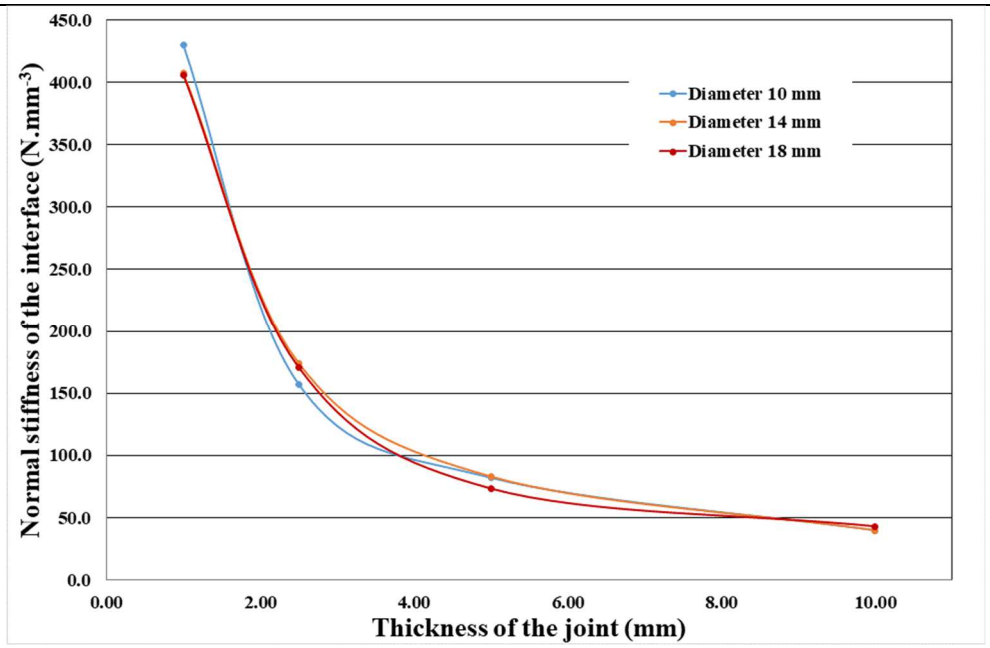

Fig.18. Normal stiffness evolution of a micro-cracked interface predicted with the KSi model and based on porosity evaluation from µCT scans.

Figure 18 shows the evolution of the normal stiffness of the micro-cracked interface as predicted by the KSi model and based on the porosity evaluation by µCT scans. The stiffnesses calculated by the model appear to be independent of the bond surface, but very strongly dependent on the bond thickness. This appears to be consistent at this level as the model is based on an asymptotic method that considers a very small thickness compared to the size of the bonded structure. The experimental

measurements show in Figure 17(d) suggest that the measured stiffness does not seem to be affected by the adhesive thickness beyond a certain surface value.

Figure 19 describes the percentage error between normal interface stiffnesses experimentally measured and those predicted by the KSi model as a function of the aspect ratio of the bonded structure. For the smallest thickness, the model shows a deviation of 15% for the D10 samples and 22% for the D14 samples. As the thickness increases, the difference between the model and the experiment increases until it reaches 80% for the three surfaces and the largest thicknesses. For the D18 samples a deviation of 85% is observed from the smallest thickness. As expected, the model gives reliable results for thin thicknesses, which is consistent with the asymptotic method of the imperfect interface model. This result is not verified for the D18 specimens, although they have an identical porosity rate. A closer view at the pore geometry in the microtomography images shows that the aspect ratio of the pores is different for the D18 samples. In fact, if the aspect ratio n, corresponding to the ratio between the small radius of the ellipsoid and the large radius of the ellipsoid $n = \frac{r}{R}$, is considered. Differences are observed, by example for samples D10 and D14 a ratio of about 0.9 is measured, whereas for sample D18 a ratio of about 0.65 is measured.

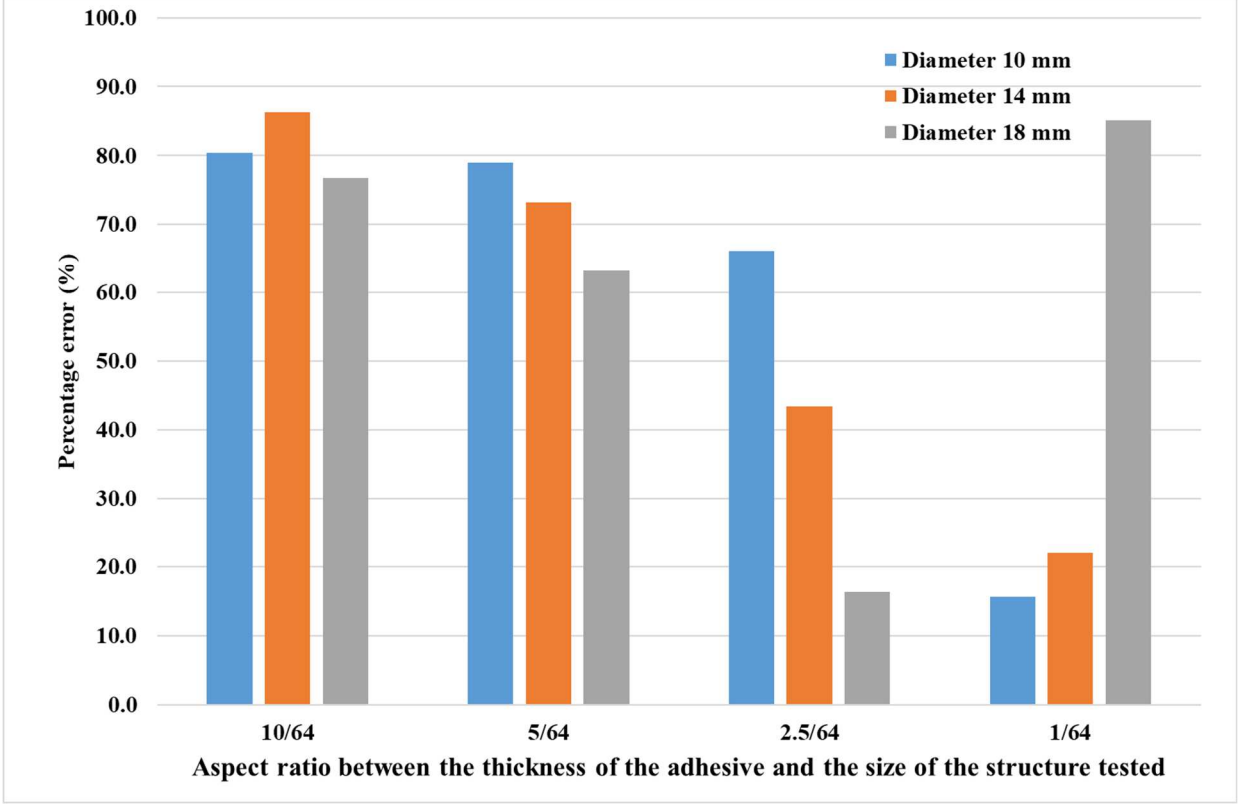

Fig.19. Percentage error for the three different diameters of bonded specimens between normal stiffnesses experimentally measured and those predicted by the KSi model as a function of the aspect ratio of the bonded structure.

5. Conclusions

The methodology presented here tests the ability of the imperfect interface model to predict the mechanical properties of the interface of a bonded connection. Several bonded specimens with different geometries were prepared and tested under controlled laboratory conditions. The mechanical properties of the SikaDur-30 adhesive were also measured by tensile tests.

Microtomographic analysis of the adhesive layer porosity in samples showed that the porosity rate was constant for all the geometries considered. It therefore appears that the porosity rate is indeed a characteristic material parameter of the adhesive.

For small thicknesses the imperfect interface model results are in good agreement with the experimental ones as expected. This result was expected. Because the imperfect interface model is based on an asymptotic method which assumes that the adhesive thickness is very small compared to the size of the bonded structure. However, it is observed that for the largest surface area the deviations are very large while the porosity rate is identical. It seems that in this case the topology of pores is measured with a larger aspect ratio, which could explain the deviation from the model. Overall porosity therefore seems to be a necessary but insufficient parameter for describing initial damage. The effect of pore topology and distribution appears to have an effect on the stiffness of the adhesive joint. In conclusion, for the moment, it seems reasonable to identify the values of these imperfect interface models by inverse identification methods, especially for large structures with complex loading.

To go further, it seems interesting to refine the description of the porosities in these models (number, orientation, topology, etc.). To better understand the variability due to the geometry of the adhesive joints and the method of implementation. Another method could be to introduce controlled defects in our bonded samples to better understand the response of the pore structure of the adhesive joint.

Acknowledgement

This project has received funding from the European Union Horizon 2020 research and innovation programme under the Marie Sklodowska-Curie grant agreement No 843218-ASSO (Adhesive Connection for Secondary Structures in Offshore wind installations).

The authors thank Messrs Luca Giuliani and Mohamed Amine Ouelhazi, master's students at the Department of Mechanical Engineering at the University of Ferrara, for their assistance during the preparation and testing of the specimens. The authors would also thank the industry BW Ideol for its financial support.

6. References

[1] Xiaocong He. A review of finite element analysis of adhesively bonded joints. International Journal of Adhesion & Adhesives 31 (2011) 248–264

[2] Adams RD, Comyn J, Wake WC. Structural adhesive joints in engineering. London: Chapman and Hall; 1998

[3] Lamberti M, Maurel-Pantel M, Ascione F, Lebon F. Influence of web/flange reinforcement on the GFRP bonded beams mechanical response: a comparison with experimental results and a numerical prediction. Compos Struct 2016;147:247–59.

[4] Lemaitre, J.; Chaboche, J.-L. Mechanics of Solid Materials; Cambridge University Press: Cambridge, UK, 1990.

[5] Lemaitre, J. A Course on Damage Mechanics; Springer: Berlin, Germany, 1992.

[6] Park, T.; Ahmed, B.; Voyiadjis, G.Z. A review of continuum damage and plasticity in concrete: Part I-Theoretical framework. Int. J. Damage Mech. 2022, 31, 901–954.

[7] Kachanov, M.L. Time of the rupture process under creep conditions. Izv. Akad. Nauk. (S.S.R.) Otd. Tech. Nauk 1958, 8, 26–31.

[8] Rabotnov, Y.N. On the Mechanism of Delayed Fracture; Izd. Akad. Nauk SSSR: Moscow, Russia, 1959; pp. 5–7.

[9] Voyiadjis, G.Z.; Kattan, P.I. Fundamental aspects for characterization in continuum damage mechanics. Int. J. Damage Mech. 2019, 28, 200–218.

[10] Li, X.; Gao, W.; Liu, W. A mesh objective continuum damage model for quasi-brittle crack modelling and finite element implementation. Int. J. Damage Mech. 2019, 28, 1299–1322.

[11] Ottosen, N.S.; Stenströ, R.; Ristinmaa, M. Continuum approach to high-cycle fatigue modeling. Int. J. Fatigue 2008, 30, 996–1006.

[12] Lindström, S.; Thore, C.; Suresh, S.; Klarbring, A. Continuous-time, high-cycle fatigue model: Validity range and computational acceleration for cyclic stress. Int. J. Fatigue 2020, 136, 105582.

[13] Suresh, S.; Lindström, S.B.; Thore, C.J.; Klarbring, A. Acceleration of continuous-time, high-cycle fatigue constrained problems in topology optimization. Eur. J. Mech. A Solids 2022, 96, 104723.

[14] Banea MD, da Silva LFM. P I Mech Eng L-J Mater 2009;223(1):1.

[15] M. Kachanov. Elastic solids with many cracks and related problems. Advances in Applied Mechanics, Vol 30, 30:259–445, 1994.

[16] I. Tsukrov and M. Kachanov. Effective moduli of an anisotropic material with elliptical holes of arbi- trary orientational distribution. International Journal of Solids and Structures, 37(41):5919–5941, 2000.

[17] M. Kachanov and I. Sevostianov. On quantitative characterization of microstructures and effective properties. International Journal of Solids and Structures, 42(2):309 – 336, 2005.

[18] I. Sevostianov and M. Kachanov. Non-interaction Approximation in the Problem of Effective Properties. In Mark Kachanov and Igor Sevostianov, editors, Effective Properties of Heterogeneous Materials, 193 of Solid Mechanics and Its Applications, pages 1– 95.

[19] C. Mauge and M. Kachanov. Effective elastic properties of an anisotropic material with arbitrarily oriented interacting cracks. Journal of the Mechanics and Physics of Solids, 42(4):561–584, 1994.

[20] Sevostianov I, Kachanov M. On some controversial issues in effective field approaches to the problem of the overall elastic properties. Mech Mater 2014;69:93–105.

[21] Fouchal F, Lebon F, Raffa ML, Vairo G (2014) An interface model including cracks and roughness applied to masonry. Open Civil Eng J 8(1):263–271

[22] Maurel-Pantel, A, Lamberti, M., Raffa, M. L, Suarez, C., Ascione, F., Lebon, F. Modelling of a GFRP adhesive connection by an imperfect soft interface model with initial damage. Composite Structures, Vol. 239, 112034, 2020.

[23] https://gbr.sika.com/en/construction/structural-strengthening/adhesives-and-bonding/structural-adhesives/sikadur-30.html

[24] J. Vicente, Y. Wyart, P. Moulin, Characterization (2d-3d) of ceramic microfiltration membrane by synchrotron radiation: new and abraded membranes, Journal of Porous Media 16 (6) (2013) 537–545. doi:10.1615/jpormedia.v16.i6.50.

[25] Maurel-Pantel, A., Voisin, M., Mazerolle, F., & Lebon, F. (2022). Comparison of three different adhesive joints using static and dynamic impact tests: Development of a new drop weight impact test rig incorporating a modified Arcan fixture. International Journal of Adhesion and Adhesives, 114, 103104.

[26] M. Cabello, J. Zurbitu, J. Renart, A. Turon, F. Martínez, A general analytical model based on elastic foundation beam theory for adhesively bonded DCB joints either with flexible or rigid adhesives. International Journal of Solids and Structures, 94, 21-34, 2016.

[27] C. Sarrado, F. A. Leone, A. Turon, Finite-thickness cohesive elements for modeling thick adhesives. Engineering Fracture Mechanics, 168, 105-113, 2016.

[28] M. Cabello, A. Turon, J. Zurbitu, J. Renart, C. Sarrado, F. Martínez, Progressive failure analysis of DCB bonded joints using a new elastic foundation coupled with a cohesive damage model. European Journal of Mechanics-A/Solids, 63, 22-35, 2017.

[29] Rekik, A., Lebon, F.: Identification of the representative crack length evolution for a multi-level interface model for quasi-brittle masonry, International Journal of Solids and Structures, Vol. 47, pp. 3011-3021, 2010.

[30] Rekik, A., Lebon, F.: Homogenization methods for interface modeling in damaged masonry, Advances in Engineering Software, Vol. 46, pp. 35-42, 2012.

[31] Bonetti, E., Bonfanti, G., Lebon, F., Rizzoni, R., A model of imperfect interface with damage, Meccanica, Vol. 52, No 8, pp. 1911–1922, 2017

[32] Lamberti, M., Maurel-Pantel, A., Lebon, F., & Ascione, F. (2022). Cyclic behaviour modelling of GFRP adhesive connections by an imperfect soft interface model with damage evolution. Composite Structures, 279, 114741.

[33] Lamberti, M., Maurel-Pantel, A., & Lebon, F. (2023). Experimental characterization and modelling of adhesive bonded joints under static and non-monotonic fracture loading in the mode II regime. International Journal of Adhesion and Adhesives, 103394.

[34] R. Hill, Elastic Properties of Reinforced Solids - Some Theoretical Principles, Journal of the Mechanics and Physics of Solids, 11(5):357-372, 1963.

[35] M.L. Raffa, Micromechanical modeling of imperfect interfaces and applications, PhD Thesis, Tor Vergata Roma 2 University and Aix-Marseille University, 2015

[36] F. Lebon, R. Rizzoni, S. Ronel-Idrissi, Asymptotic analysis of some non-linear soft thin layers, Computers and Structures, 82:1929–1938, 2004

[37] M.L. Raffa, F. Lebon, R. Rizzoni, Derivation of a model of imperfect interface with finite strains and damage by asymptotic techniques: an application to masonry structures, 53:1645–1660, 2018

Appendix 1: Homogenization of micro-cracked materials

The imperfect interface model presented in this paper is derived starting from a heterogeneous interphase, comprising an elastic material in which a microstructure is embedded. This appendix focuses on this kind of interphase materials. In our technique, the homogenization of this heterogeneous material follows a micromechanical approach. Usually, the homogenization techniques for microcracked media have been derived from more general formulations for dry pores, voids, cracks, etc. of various shapes, e. g. spherical, ellipsoidal, cylindrical, etc. The non-interaction approximation (NIA) to the problem of effective properties of a heterogeneous material considers that interactions between inhomogeneities are neglected. In the NIA micromechanical approach, a microstructural parameter is introduced, which gives a measure of the microcracks density (e.g. volume fractions). In order to determine the effective elastic properties of the heterogeneous material with voids (pores, cracks) and under the assumptions of linear elasticity and small perturbation, it is considered that on a Representative Elementary Volume (REV) of the material, the local second-order strain tensor $\varepsilon(u)$ is given by [34]:

$$\varepsilon(u) = S^0 : \sigma^0 + \Delta\varepsilon$$

where S^0 is the fourth-order compliance tensor of the matrix (without voids), σ^0 the macroscopic applied second-order stress tensor and $\Delta\varepsilon$ the additional strain due to the presence of voids. The material is assumed to be linear elastic, thus the additional strain due to the voids is a linear function of the applied stress:

$$\Delta\varepsilon = H : \sigma^0$$

where H is a fourth-order *compliance contribution tensor* of the inhomogeneity. Generally speaking, the H tensor depends on the material, the void density and the shape of the voids. This kind of approach is also called *stress-based approach*. It can be proved for a simple crack γ that:

$$\Delta\varepsilon = \frac{1}{V}\oint_{\gamma} [v] \otimes^s \boldsymbol{n}\, dS$$

where, V is the REV volume, **n** is the normal unit vector of the crack surface, $\otimes^s$ is the symmetric tensorial product, and $[\boldsymbol{v}]$ is the displacement discontinuity vector along γ. Note that for a planar crack, the additional strain becomes:

$$\Delta\varepsilon = \frac{[\boldsymbol{\gamma}]}{V} < [v] > \otimes^s \boldsymbol{n}$$

where <> is the average along γ. For a uniform macroscopic stress, the additional term can be written as:

$$H{:}\,\sigma^0 = \frac{[\boldsymbol{\gamma}]}{V} B\sigma^0 \boldsymbol{n}$$

where B is a second-order tensor which links $< [v] >$ to the macroscopic stress. As H, the tensor B depends on the material, the void density and the shape of the voids.

As an example, in the three-dimensional case of an isotropic material weakened by a penny-shaped void of radius b (see Figure 20), the last equation reads [15]:

$$H{:}\,\sigma^0 = \frac{16\left(1-\nu_0^2\right)}{3\left(1-\frac{\nu_0}{2}\right)E_0}\rho((\boldsymbol{n}\otimes\boldsymbol{n}).\sigma^0 - \nu_0\ (\boldsymbol{n}\otimes\boldsymbol{n}\otimes\boldsymbol{n}\otimes\boldsymbol{n}){:}\,\sigma^0)$$

where E_0 and ν_0 are the Young's modulus and the Poisson's ratio of the sane material, respectively, and ρ is the crack density [17], defined as:

$$\rho = \frac{b^3}{V}$$

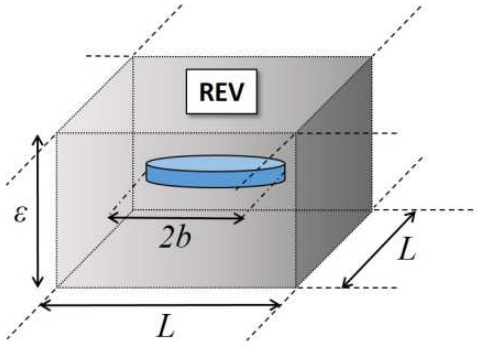

Figure 20: Penny-shape crack (from [35])

In conclusion, it can be proved that the coefficients of the second-order stiffness tensor C (the inverse of the compliance tensor, i.e. which links the stress to the strain; $C = (S^0+H)^{-1}$) of the material containing voids are of the form

$$C_{ij} = \frac{C_{ij}^0}{1 + R_{ij}\rho}$$

where the coefficients R_{ij} depends on the material and the shape of the voids.

Appendix 2: Derivation of interface laws by asymptotic expansions for soft materials

A thin layer with cross-section S and uniform small thickness $\varepsilon \ll 1$ is considered. The thin layer (interphase) is embedded between two bodies, named as adherents. The thin layer is supposed to be perfectly bonded to the adherents. The material in the thin layer is a microcracked material as defined in appendix 1. Classically, the layer being thin, it is natural to study the problem where the small thickness tends to zero and to replace the thin interphase by a surface (interface) whose is the interphase geometrical limit.

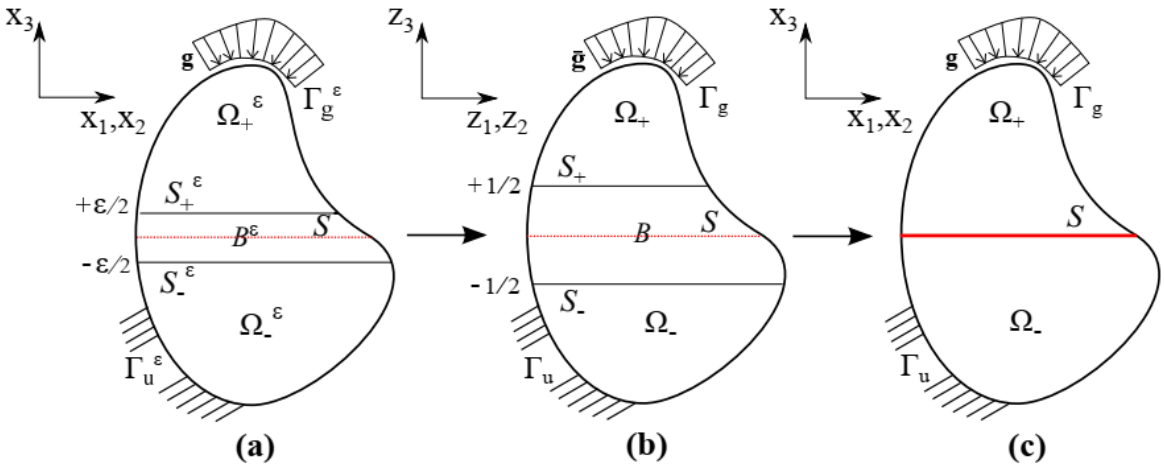

Figure 21: Asymptotic procedure (from [35]), from interphase to interface

The study is done in five steps [36,37]:

1. Asymptotic expansions of the mechanical fields (displacements, stress tensor, strain, tensor, etc.) with respect to the thickness.
2. Rescaling (from (a) to (b) in Figure 21). A blow up of the thin layer is done in the direction normal to the thickness surface.
3. Analysis of the equilibrium equations in the adherents and in the adhesive using expansions. The terms of each order of expansion are identified.
4. Matching linking initial and rescaled configurations.
5. Obtention of a model of interface on the final configuration (c in figure 21).

In this work, a homogenized microcracked material is considered (Figure 22). The volume of the REV is given by V = εS. Note that, in appendix 1, Figure 20, S=L^2). In this case, the asymptotic expansion of tensor *C* has been found resulting in a soft material:

$$C = \varepsilon C^1 + O(\varepsilon)$$

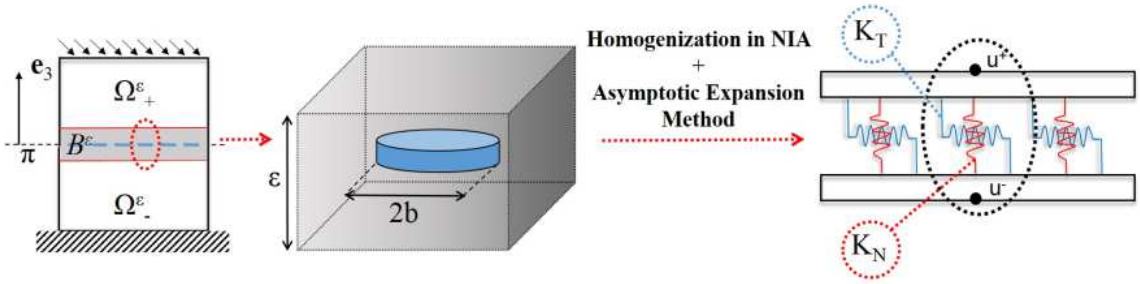

Figure 22: Sketch of the method (from [35])

In this case, using expansions, the interface is replaced by an interface equivalent to a sequence of normal and tangential springs. The stress vector $\sigma.n$ is linked to the jump in the displacement along the interface *[u]* by:

$$\sigma.n = K(b)[u]$$

where K = diag (K_N, K_T, K_T) with

$$K_N = \frac{3E_0S}{16\,b^3(1-\nu_0^2)};\; K_T = \frac{3E_0S(1-\nu_0)}{32\,b^3(1-\nu_0^2)}$$